Zenith/Nadir Pointing mm-Wave Radars: Linear or Circular Polarization?

Michele Galletti, Dong Huang, and Pavlos Kollias

***Abstract*—We consider zenith/nadir pointing atmospheric radars and explore the effects of different dual-polarization architectures on the retrieved variables: reflectivity, depolarization ratio, cross-polar coherence, and degree of polarization. Under the assumption of azimuthal symmetry, when the linear depolarization ratio (LDR) and circular depolarization ratio (CDR) modes are compared, it is found that for most atmospheric scatterers reflectivity is comparable, whereas the depolarization ratio dynamic range is maximized at CDR mode by at least 3 dB. In the presence of anisotropic (aligned) scatterers, that is, when azimuthal symmetry is broken, polarimetric variables at CDR mode do have the desirable property of rotational invariance and, further, the dynamic range of CDR can be significantly larger than the dynamic range of LDR. The physical meaning of the cross-polar coherence is revisited in terms of scattering symmetries, that is, departure from reflection symmetry for the LDR mode and departure from rotation symmetry for the CDR mode. The Simultaneous Transmission and Simultaneous Reception mode (STSR mode or hybrid mode or $Z_{\rm DR}$ mode) is also theoretically analyzed for the case of zenith/nadir pointing radars and, under the assumption of azimuthal symmetry, relations are given to compare measurements obtained at hybrid mode with measurements obtained from orthogonal (LDR and CDR) modes.**

***Index Terms*—Circular depolarization ratio (CDR), circular polarization, degree of polarization, linear depolarization ratio (LDR), linear polarization, polarization response, reflectivity.**

I. Introduction

THE OPERATIONAL implementation of polarimetry in radar systems for atmospheric remote sensing has seen a considerable development in the last years [1]–[3]. After the *American Recovery and Reinvestment Act of 2009*, the Atmospheric Radiation Measurement (ARM) Climate Research Facility of the United States Department of Energy [4], [5] was retrofitted with a diverse array of radar systems at different frequencies and polarizations. Examples are the ARM zenith-pointing dual-polarization radar systems, like the W-band ARM Cloud Radar (WACR), the decommissioned Millimeter Wave Cloud Radar (MMCR) [6] and the Ka-band Zenith-pointing Radar (KaZR). The WACR and the KaZR systems operate at W and Ka band, respectively; they transmit linear polarization and receive the copolar and cross-polar components of the backscattered signal. In the following, this polarimetric mode (linear polarization transmission, co- and cross-pol receive) is termed linear depolarization ratio (LDR) mode. The MMCR operated at Ka band (35 GHz), transmitted circular polarization and received the copolar and cross-polar components of the backscattered signal. Such operating mode is indicated with circular depolarization ratio (CDR) mode.

Since most atmospheric scatterers tend to have a shape close to spherical, both LDR and CDR modes are characterized by a large difference in signal power (generally larger than 20 dB) between the two receive polarimetric channels. This circumstance limits the domain of applicability of polarimetry to those regions of the scanned space whose signals are both within the acceptable receiver dynamic range, and has therefore spawned the use of transmit polarization states that are not copolar and cross-polar with respect to the receive channels. Whenever the receive polarization states are not copolar and cross-polar with respect to the transmit polarization, the polarization architecture is referred to as "hybrid". An example of hybrid architecture is the so-called $Z_{\rm DR}$ mode (differential reflectivity mode, also known as Simultaneous Transmission Simultaneous Reception mode (STSR) implemented in the US NEXRAD network and in the ARM X-SACR radar.

In this paper, we only consider the LDR, CDR, and $Z_{\rm DR}$ modes for implementation in zenith/nadir pointing atmospheric radars. However, other polarimetric architectures were proposed and implemented, specifically for the characterization of ice particles by hemispheric-scanning millimeter-wave radars. Such polarimetric operating modes are the SLDR mode (slant linear depolarization ratio mode), that makes use of slant linear polarization on transmission and receives the signal in the copolar and cross-polar channels ($+45^\circ$ and -45° linear polarization); the SLDR* mode (slant quasi-linear depolarization ratio mode) and the EDR mode (elliptical depolarization ratio mode), that makes use of elliptical polarization on transmission and receives the signal in the copolar and cross-polar channels [7]–[9].

The purpose of this paper is twofold: in the context of zenith-pointing atmospheric radars (i.e., when azimuthal symmetry can be assumed), we first investigate the pros and cons of the LDR and CDR polarimetric modes; then, we develop a theoretical framework that provides algebraic relations between variables retrieved at LDR mode, CDR mode and simultaneous transmission ($Z_{\rm DR}$ mode). Azimuthal symmetry is expected for most distributions of hydrometeors at zenith/nadir observation angles like pristine crystals, melting and/or rimed aggregates, droxtals, cloud droplets and raindrops. The presence of aligned

Manuscript received February 23, 2012; revised August 6, 2012, October 16, 2012, and November 27, 2012; accepted January 15, 2013. Date of publication March 7, 2013; date of current version November 26, 2013. This work was supported by the Brookhaven National Laboratory LDRD program and by the Atmospheric Science Research (ASR) program of the U.S. Department of Energy.

The authors are with the Brookhaven National Laboratory, Radar Science Group, Upton, NY 11973-5000 USA (e-mail: mgalletti@bnl.gov; dhuang@bnl.gov; pavlos.kollias@mcgill.ca).

Color versions of one or more of the figures in this paper are available online at http://ieeexplore.ieee.org.

Digital Object Identifier 10.1109/TGRS.2013.2243155

scatterers (due to electrification or wind-shear for example) breaks the assumption of rotation symmetry, and, consequently, azimuth symmetry. Ideally, the verification of this assumption involves the analysis of the cross-polar coherence from dual-polarization radars operating at both LDR and CDR modes. The cross-polar coherence at horizontal polarization transmit (also known in the weather radar literature as cross-polar correlation coefficient and indicated with $\rho_{\rm xh}$ or $\rho_{\rm xv}$ [10], [11]) departs from zero if and only if the target departs from reflection symmetry [12]. This may be due to aligned hydrometeors in a direction other than the two orthogonal directions corresponding to the antenna ports. The cross-polar coherence at circular polarization transmit (also known in the weather radar literature as ORTT, Orientation Parameter) indicates departure from rotation symmetry, due to the presence of aligned hydrometeors, in whatever alignment direction in the polarization plane (regardless of the antenna ports orientation). If a target possesses both reflection and rotation symmetry, it is said to have azimuthal symmetry.

The potential of the polarimetric approach for the characterization of ice cloud microphysics can be better appreciated from ground-based radar systems, thanks to their superior radiometric, spatial and spectral resolution. Scatterers with azimuthal symmetry only have two degrees of freedom, generally represented through reflectivity, related to the backscatter cross-section per unit volume, and the depolarization ratio, that also accounts for properties of the scatterers' shape. In the particular zenith-pointing geometry, the polarimetric information can be used to infer the shape of scatterers in terms of how "sphere-like" versus how "needle-like" they appear to the probing wavelength. Depending on the width of the canting angle distribution, millimeter wave polarimetry at zenith/nadir has demonstrated the capability of distinguishing quasi-spherical scatterers (drizzle droplets, very small hexagonal ice crystals) from planar (plates, stellars, dendrites), and from columnar (columns, needles) ice crystals [9]. Mm-wavelength polarimetry also brings insight to the characterization of non-axisymmetric oscillations of raindrops and break-up processes [17]–[21] and is very effective in the discrimination of atmospheric scatterers (hydrometeors) from atmospheric plankton (birds, bugs, bats, suspended particles), the latter appearing with larger depolarization ratio values [22], [23].

The theoretical development of Section III considers scatterers with azimuthal symmetry and illustrates how the reduced degrees of freedom are represented in the Covariance and Mueller matrices. Since for scatterers with azimuthal symmetry a dual-pol system retrieves the same information as a fully polarimetric system, the target representation is translated from the Covariance or Mueller matrices into the Coherency matrix (measurable by a dual-pol system). With an ideal dual-polarization radar system (noiseless and perfect cross-polar isolation), transmission of linear polarization is theoretically equivalent to the transmission of circular polarization since $Z_{\rm C}$ and CDR can be retrieved from $Z_{\rm H}$ and LDR and vice-versa. However, the returned power is diversely distributed in the copolar and cross-polar channels for the two polarization bases. This effect has a small (and indeed negligible) impact on the reflectivity factor, and a more significant impact on the depolarization ratio (maximized at circular polarization transmit by at least 3 dB). When the finite sensitivity and finite cross-polar isolation of the radar system are taken into account, CDR mode emerges as a better option than LDR mode.

Two considerations hold for scatterers with azimuthal symmetry:

- The difference between reflectivity at linear and reflectivity at circular polarization is always less than 0.5 dBZ for scatterers with intrinsic $CDR < -6$ dB (0.5 dBZ is the nominal error associated with reflectivity measurements of ARM radars), so, implementation of CDR mode does not appreciably degrade the sensitivity of the system.
- CDR is always larger than LDR by at least 3 dB [13]; considering that the lower bound is the same (see Section IV) for antennas with the same cross-polar isolation, we conclude that CDR mode offers a larger dynamic range for depolarization ratio measurements.

In absence of azimuth symmetry, that is, in presence of aligned scatterers, polarimetric variables obtained at circular polarization (reflectivity, depolarization ratio, cross-polar coherence, degree of polarization) have a physical meaning that is more pertinent to the geometry of the problem, since they are independent from the specific alignment direction (with respect to the antenna ports) of the anisotropic scatterers potentially present in the radar resolution volume. Further, the presence of anisotropic scatterers additionally enhances the dynamic range of CDR with respect to the dynamic range of LDR [26].

After the analysis of the orthogonal modes (LDR and CDR modes), we theoretically consider simultaneous transmission (generally employed in operational scanning precipitation radars) also for zenith/nadir pointing atmospheric radars. In particular, the ARM program utilizes simultaneous transmission for one of its hemispheric scanning radars (X-SACR). Under the assumption of azimuthal symmetry, we work out the mathematical relations between variables at LDR and CDR modes and variables at simultaneous transmission ($Z_{\rm DR}$ mode). With respect to orthogonal modes (LDR and CDR modes), $Z_{\rm DR}$ mode has the advantage that the domain of applicability of polarimetry is larger, since both polarimetric channels receive comparable power levels. The drawbacks are a 3 dB drop in sensitivity, higher requirements in antenna cross-polar isolation [27]–[30] and a potential bias in polarimetric variables due to non-uniform beam filling [31].

II. Theoretical Background

We redefine the known polarimetric variables not simply as scalar quantities, but as maps defined on the surface of the Poincare sphere, parameterized by the orientation angle ψ and the ellipticity angle χ. The two angles that parameterize the surface of the Poincare sphere identify a point on the surface that corresponds to a specific polarization state (that we denote with x)

$$(\psi, \chi) \leftrightarrow (x). \tag{1}$$

Together with the polarization state corresponding to the antipodal point (that we denote with y), the pair of orthogonal

polarization states (x,y) constitutes an orthogonal polarization basis.

We define the Reflectivity Poincare map as that map that associates to every point of the Poincare sphere surface the maximum returned power (either copolar or cross-polar)

$$Z(\psi,\chi) \propto max\left[\left\langle|s_{xx}|^2\right\rangle, \left\langle|s_{yx}|^2\right\rangle\right]. \tag{2}$$

Depending on the transmitted polarization, we obtain the reflectivity at horizontal transmit: $Z(0^\circ, 0^\circ) = Z_{\rm H}$; reflectivity at vertical transmit: $Z(90^\circ, 0^\circ) = Z_{\rm V}$; and reflectivity at circular transmit $Z(0^\circ, \pm 45^\circ) = Z_{\rm C}$.

The Depolarization Ratio Poincare map is defined as the map that associates to every point of the Poincare sphere the ratio of minimum to maximum returned power (e.g., cross-to-copolar power ratio for linear polarization transmit, or co-to-cross-polar power ratio for circular polarization transmit) [9]

$$DR(\psi,\chi) \equiv \frac{min\left[\left\langle|s_{xx}|^2\right\rangle, \left\langle|s_{yx}|^2\right\rangle\right]}{max\left[\left\langle|s_{xx}|^2\right\rangle, \left\langle|s_{yx}|^2\right\rangle\right]}. \tag{3}$$

For example, for horizontal polarization transmit we have that $DR(0^\circ, 0^\circ) = LDR_{\rm H}$, for vertical polarization transmit we have $DR(90^\circ, 0^\circ) = LDR_{\rm V}$, for slant 45° linear polarization transmit we have $DR(\pm 45^\circ, 0^\circ) = SLDR$, for circular polarization transmit we have $DR(0^\circ, \pm 45^\circ) = CDR$. Elliptical polarization on transmission was proposed in [8], and the corresponding depolarization ratio is referred to as elliptical depolarization ratio (EDR), so that $DR(0^\circ, \pm 40^\circ) = EDR$. The concept of depolarization ratio Poincare map encompasses all these polarimetric variables in one single entity. Follows that reflectivity at horizontal transmit $Z_{\rm H}$, and the linear depolarization ratio LDR are, respectively defined as

$$Z_H \propto \left\langle|s_{hh}|^2\right\rangle \tag{4}$$

$$LDR \equiv \frac{\left\langle|s_{vh}|^2\right\rangle}{\left\langle|s_{hh}|^2\right\rangle}. \tag{5}$$

The reflectivity at circular transmit $Z_{\rm C}$ and the circular depolarization ratio CDR are, respectively defined as:

$$Z_C \propto \left\langle|s_{LR}|^2\right\rangle \tag{6}$$

$$CDR \equiv \frac{\left\langle|s_{RR}|^2\right\rangle}{\left\langle|s_{LR}|^2\right\rangle}. \tag{7}$$

The cross-polar coherence Poincare map is defined as the map that associates to every point of the Poincare sphere the normalized correlation coefficient between the copolar and cross-polar returns

$$\rho_{cx}(\psi,\chi) \equiv \frac{\left|\left\langle s_{xx}s_{yx}^*\right\rangle\right|}{\sqrt{\left\langle|s_{xx}|^2\right\rangle\left\langle|s_{yx}|^2\right\rangle}}. \tag{8}$$

At horizontal/vertical polarization transmit, the cross-polar coherence has appeared in the literature with the name of cross-polar correlation coefficient, and has generally been indicated with the symbols $\rho_{\rm xh}$ and $\rho_{\rm xv}$ [10], [11]. The cross-polar correlation coefficient departs from zero if and only if the target departs from reflection symmetry [12]. At circular polarization, the cross-polar coherence has appeared in the literature with the name of orientation parameter, indicated with the symbol ORTT. The orientation parameter departs from zero if and only if the target departs from rotation symmetry [1].

The copolar coherence Poincare map is the normalized correlation coefficient between the copolar returns of the two orthogonal polarization states

$$\rho_{co}(\psi,\chi) \equiv \frac{\left|\left\langle s_{xx}s_{yy}^*\right\rangle\right|}{\sqrt{\left\langle|s_{xx}|^2\right\rangle\left\langle|s_{yy}|^2\right\rangle}}. \tag{9}$$

At horizontal/vertical polarization transmit, the copolar coherence has been referred to as copolar correlation coefficient, generally indicated with $\rho_{\rm hv}$, and has been extensively studied [1].

The degree of polarization Poincare map is defined as

$$p(\psi,\chi) \equiv \sqrt{1 - \frac{4\left[\left\langle|s_{xx}|^2\right\rangle\left\langle|s_{yx}|^2\right\rangle - \left|\left\langle s_{xx}s_{yx}^*\right\rangle\right|^2\right]}{\left[\left\langle|s_{xx}|^2\right\rangle + \left\langle|s_{yx}|^2\right\rangle\right]^2}}. \tag{10}$$

For a general target, an algebraic relation holds between the Poincare maps of degree of polarization, depolarization ratio and cross-polar coherence

$$\left[1 - p^2(\psi,\chi)\right] = \frac{4DR(\psi,\chi)}{\left[1 + DR(\psi,\chi)\right]^2}\left[1 - \rho_{cx}^2(\psi,\chi)\right]. \tag{11}$$

In particular, if horizontal polarization is used, the relation above reduces to

$$\left(1 - p_H^2\right) = \frac{4LDR}{\left[1 + LDR\right]^2}\left(1 - \rho_{xh}^2\right) \tag{12}$$

where $p_{\rm H}$ is the degree of polarization at horizontal transmit, LDR is the linear depolarization ratio, and $\rho_{\rm xh}$ is the cross-polar correlation coefficient. If the target has reflection symmetry, then $\rho_{\rm xh} = 0$, and the relation above simplifies to

$$p_H = \frac{1 - LDR}{1 + LDR}. \tag{13}$$

If circular polarization is used, the relation in (11) reduces to

$$\left(1 - p_C^2\right) = \frac{4CDR}{\left[1 + CDR\right]^2}(1 - ORTT^2) \tag{14}$$

where $p_{\rm C}$ is the degree of polarization at circular transmission, CDR is the circular depolarization ratio, and ORTT is the orientation parameter. If the target has rotation symmetry, like it is often the case for zenith/nadir pointing mm-wave radars, then $ORTT = 0$, and the relation above simplifies to

$$p_c = \frac{1 - CDR}{1 + CDR}. \tag{15}$$

Scatterers that exhibit both reflection and rotation symmetry are said to have azimuthal symmetry. For scatterers with azimuthal symmetry, the cross-polar correlation coefficients at horizontal and vertical polarizations ($\rho_{\rm xh}$ and $\rho_{\rm xv}$) and the cross-polar correlation coefficient at circular polarization (ORTT, orientation

parameter) are zero, and, consequently, the cross-polar coherence Poincare map is zero everywhere

$$\rho_{cx}(\psi,\chi)=0. \tag{16}$$

For scatterers with azimuthal symmetry, the relation in (11) reduces to

$$p(\psi,\chi)=\frac{1-DR(\psi,\chi)}{1+DR(\psi,\chi)}. \tag{17}$$

For scatterers with azimuthal symmetry, there is a one-to-one relation between the degree of polarization and the depolarization ratio that holds for every polarization basis (17).

The cross-polar coherence can be used to verify the assumption of scattering symmetries, namely reflection, rotation and azimuth symmetry: the cross-polar coherence at horizontal or vertical transmit (cross-polar correlation coefficients $\rho_{\rm xh}$ or $\rho_{\rm xv}$) accounts for departure from reflection symmetry, the cross-polar coherence at circular transmit (ORTT, orientation parameter) accounts for departure from rotation symmetry; the cross-polar coherence is zero everywhere on the Poincare sphere if and only if the target possesses azimuth symmetry. The degree of polarization is redundant with respect to the depolarization ratio and the cross-polar coherence, as indicated by (11), (12), and (14). However, when propagation effects and finite cross-polar isolation of the antenna are taken into account, use of the degree of polarization at horizontal or vertical transmit does have significant advantages [36].

If for centimeter-wavelength scanning precipitation radars (X, C, S bands) operating at simultaneous transmission ($Z_{\rm DR}$ mode) reflection symmetry of the scatterers is assumed, in mm-wave radar polarimetry at zenith/nadir, azimuth symmetry (i.e., reflection plus rotation symmetry) is generally assumed.

III. Azimuthal Symmetry

A. Covariance Matrix

Distributed scatterers with azimuthal symmetry only have two independent parameters.

At circular basis, considering that copolar returns are the same at right-hand and left-hand circular transmit, the corresponding covariance matrix is given by:

$$\Sigma^{C}_{BSA}=\begin{bmatrix}\langle|s_{RR}|^2\rangle & 0 & 0\\ 0 & 2\langle|s_{LR}|^2\rangle & 0\\ 0 & 0 & \langle|s_{RR}|^2\rangle\end{bmatrix}. \tag{18}$$

At linear polarization, considering that copolar returns at horizontal and vertical polarizations are equal ($Z_{\rm DR}=0$ dB), the corresponding covariance matrix is given by:

$$\Sigma^{L}_{BSA}=\begin{bmatrix}\langle|s_{hh}|^2\rangle & 0 & \langle s_{hh}s^*_{vv}\rangle\\ 0 & 2\langle|s_{vh}|^2\rangle & 0\\ \langle s^*_{hh}s_{vv}\rangle & 0 & \langle|s_{hh}|^2\rangle\end{bmatrix}. \tag{19}$$

In (19) the off-diagonal term is real and not independent from the diagonal terms. This implies that the backscatter differential phase ($\delta_{\rm co}$) is either 0° or 180°, and that the following relation holds

$$\langle s_{hh}s^*_{vv}\rangle=\langle|s_{hh}|^2\rangle-2\langle|s_{vh}|^2\rangle. \tag{20}$$

The relation in (20) holds in general for targets with azimuthal symmetry, and can be easily proven by considering the relations to obtain the 1,3 element of the covariance matrix at circular polarization from measurements at horizontal/vertical basis (see [1, eq. 3.196c]). For scatterers with azimuth symmetry, the copolar correlation coefficient $\rho_{\rm hv}$, defined as

$$\rho_{hv}\equiv\frac{|\langle s_{hh}s^*_{vv}\rangle|}{\sqrt{\langle|s_{hh}|^2\rangle\langle|s_{vv}|^2\rangle}} \tag{21}$$

is not independent from LDR. For $0\le LDR\le 0.5$ (linear units) that is, $-\infty$dB $\le LDR\le -3$ dB the following relation holds:

$$\rho_{hv}=1-2LDR. \tag{22}$$

For targets with $0.5\le LDR\le 1$, that is, -3 dB $\le LDR\le 0$ dB the following relation holds:

$$\rho_{hv}=2LDR-1. \tag{23}$$

Indeed, the two degrees of freedom of a target with azimuthal symmetry can be completely described by one power-related variable, like reflectivity at horizontal transmit $Z_{\rm H}$ or reflectivity at circular transmit $Z_{\rm C}$ or the trace of the coherency matrix, and by one power-independent variable that can equivalently be chosen among LDR, CDR, $p_{\rm H}$, $p_{\rm C}$ or $\rho_{\rm hv}$.

A property of the covariance matrix is that the trace is invariant under polarization bases transformations; simple algebra yields the following relation:

$$Trace[\Sigma_{BSA}]\propto Z(\psi,\chi)\left[1+DR(\psi,\chi)\right]. \tag{24}$$

In turn, (24) yields

$$Z_H[1+LDR]=Z_C[1+CDR]. \tag{25}$$

The considerations above clearly show that, for scatterers with azimuthal symmetry, measurements from a fully polarimetric system yielding the Covariance matrix do not contain more information than measurements from a dual-polarization system yielding the Coherency matrix $\mathbf{J}$

$$\boldsymbol{J}_H=\begin{bmatrix}\langle|s_{hh}|^2\rangle & 0\\ 0 & \langle|s_{vh}|^2\rangle\end{bmatrix} \tag{26}$$

$$\boldsymbol{J}_C=\begin{bmatrix}\langle|s_{RR}|^2\rangle & 0\\ 0 & \langle|s_{LR}|^2\rangle\end{bmatrix}. \tag{27}$$

Under the assumption of azimuthal symmetry, dual-polarization measurement of the coherency matrix at a given transmit polarization can be translated into the corresponding covariance matrix, rotated to a new basis, and reduced to the Coherency matrix in the new polarization basis. The theoretical conclusion is that dual-polarization zenith/nadir pointing radars illuminating scatterers with azimuthal symmetry can apparently implement either the LDR or the CDR mode, and

still retrieve equivalent information. However, even though azimuthal symmetry guarantees that the trace of the Coherency matrix is the same for linear and circular polarization bases, the power is diversely distributed in the copolar and cross-polar channels.

B. Mueller Matrix

Under the assumption of azimuthal symmetry, the Mueller matrix can in general be written in terms of Huynen parameters as [3], [37]

$$K_{az} = \begin{bmatrix} A_0 + B_0 & 0 & 0 & 0 \\ 0 & A_0 & 0 & 0 \\ 0 & 0 & A_0 & 0 \\ 0 & 0 & 0 & -A_0 + B_0 \end{bmatrix}. \quad (28)$$

A_0 and B_0 are always non-negative by definition [3]; the total backscattered power from a fully polarimetric system (trace of the covariance matrix Σ_{BSA}) and the total backscattered power from a dual-polarization system (trace of the coherency matrix **J**) are given by:

$$Trace[\Sigma_{BSA}] = 2\,Trace[\boldsymbol{J}] = 2(A_0 + B_0). \quad (29)$$

The Mueller matrix contains the same information as the Covariance matrix, but has the advantage that it actually maps incident partially polarized Stokes vectors into backscattered partially polarized Stokes vectors. The degree of polarization Poincare map can then be obtained analytically

$$p(\psi, \chi) = \frac{\sqrt{A_0^2 \cos^2(2\chi) + (A_0 - B_0)^2 \sin^2(2\chi)}}{A_0 + B_0}. \quad (30)$$

Equation (30) holds in general, with the only assumption of target azimuthal symmetry, but no assumption on the scattering regime (Rayleigh versus non-Rayleigh). Further, for scatterers with azimuthal symmetry, the degree of polarization maps one-to-one to the depolarization ratio (17). Consequently, the difference between reflectivity at linear and reflectivity at circular polarization can also be evaluated. The study of (30) yields all the answers relative to the depolarization properties of scatterers with azimuthal symmetry.

1) Case 1: $A_0 \geq B_0$—From Spheres to Dipoles: This case is what most frequently occurs in atmospheric radar signatures, and was first analyzed in [13]. The parameter B_0 varies between 0 and A_0 (that is, CDR varies between 0 and 1, linear units). The degree of polarization at horizontal transmit is in general given by

$$p_H = \frac{A_0}{A_0 + B_0} \quad (31)$$

from which we have that

$$LDR = \frac{B_0}{2A_0 + B_0}. \quad (32)$$

The degree of polarization at circular transmit is given by

$$p_c = \frac{A_0 - B_0}{A_0 + B_0}. \quad (33)$$

CDR is given by

$$CDR = \frac{B_0}{A_0}. \quad (34)$$

The degree of polarization at linear transmit is always equal to or greater than the degree of polarization at circular transmit ($p_{\rm H} \geq p_{\rm C}$). This implies that the reflectivity at linear transmit is always equal to or greater than the reflectivity at circular transmit ($Z_{\rm H} \geq Z_{\rm C}$), and that the depolarization ratio at linear transmit is always equal to or lower than the depolarization ratio at circular transmit (LDR $\leq$ CDR). Equality is obtained for $B_0 = 0$, for which $Z_{\rm H} = Z_{\rm C}$, $LDR = CDR = 0$ (linear units) and $p_{\rm H} = p_{\rm C} = 1$. In this case ($B_0 = 0$), corresponding to a cloud of spheres, the degree of polarization equals 1 for every transmit polarization state [Fig. 4(a)]

$$p(\psi, \chi) = 1. \quad (35)$$

For $B_0 = A_0$ the degree of polarization varies between a minimum of 0 (circular polarization) and a maximum of 0.5 (linear polarization). This corresponds to a cloud of randomly oriented dipoles with degree of polarization Poincare map given by Fig. 4(b)

$$p(\psi, \chi) = \frac{\cos(2\chi)}{2}. \quad (36)$$

In this case we have that $CDR = 0$ dB and $LDR = -4.77$ dB; further, $Z_{\rm H}$ is greater than $Z_{\rm C}$ by 1.76 dBZ (Fig. 1).

Even though for a cloud of randomly oriented dipoles the difference between $Z_{\rm H}$ and $Z_{\rm C}$ is larger than the nominal uncertainty of 0.5 dBZ associated with reflectivity measurements, we also note that for most scatterers of interest in mm-wave radar meteorology the actual difference in reflectivity at linear and circular polarization is smaller. In Fig. 2(a), the difference betweeh $Z_{\rm H}$ and $Z_{\rm C}$ is expressed as a function of intrinsic CDR of the target. For scatterers with $CDR < -10$ dB, the difference in reflectivity is approximately smaller than 0.2 dBZ and is therefore negligible. For dipole-like scatterers with $CDR > -6$ dB (that, indeed, seldom occur in the atmosphere) the difference exceeds 0.5 dBZ. On the other hand, the difference between CDR and LDR is never negligible and it always exceeds 3 dB. The difference tends to exactly 3 dB as the scatterers tend to the spherical shape [Fig. 2(b)].

To reinforce these ideas we carried out simple T-matrix simulations [32]–[34] of monodispersed 3-D randomly oriented spheroids (for $D = 2$ and 6 mm, representing oscillating raindrops) and of monodispersed 3-D randomly oriented columnar ice crystals (Length $= 2$ mm, Diameter $= 0.4$ mm) to qualitatively assess the order of magnitude of these differences. The distributions of particles are 3-D randomly oriented and do not account for the fact that hydrometeors tend to fall with their major axis aligned in the horizontal plane. The results are reported in Table I, and indicate that the difference between reflectivity at linear and circular polarizations is of the order of some tenths of dBZ, and is probably negligible. The same is not true for the depolarization ratio, where CDR always exceeds LDR by at least 3 dB.

2) Case 2: $A_0 < B_0$—From Dipoles to Helices: This class of scatterers is hardly ever found in the natural atmosphere. For

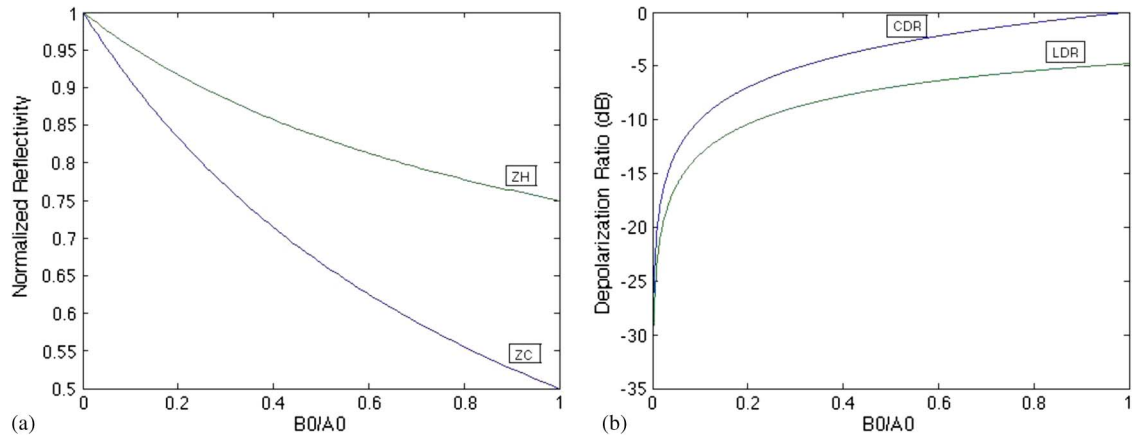

Fig. 1. Case 1, $A_0 \geq B_0$ from spheres to dipoles: On the abscissa is B_0/A_0 (equivalent to CDR in linear units) ranging from 0 (cloud of spheres) to 1 (cloud of randomly oriented dipoles). Left: on the ordinate is the Reflectivity normalized to the 1, 1 term of the Mueller matrix (trace of the coherency matrix). For this class of targets (azimuthal symmetry with $A_0 > B_0$), reflectivity at horizontal transmission is always larger than reflectivity at circular transmission, generally by a negligible amount. Right: on the ordinate is the Depolarization Ratio (in dB). For this class of targets (azimuthal symmetry with $A_0 > B_0$) the dynamic range of CDR is always larger than the dynamic range of LDR.

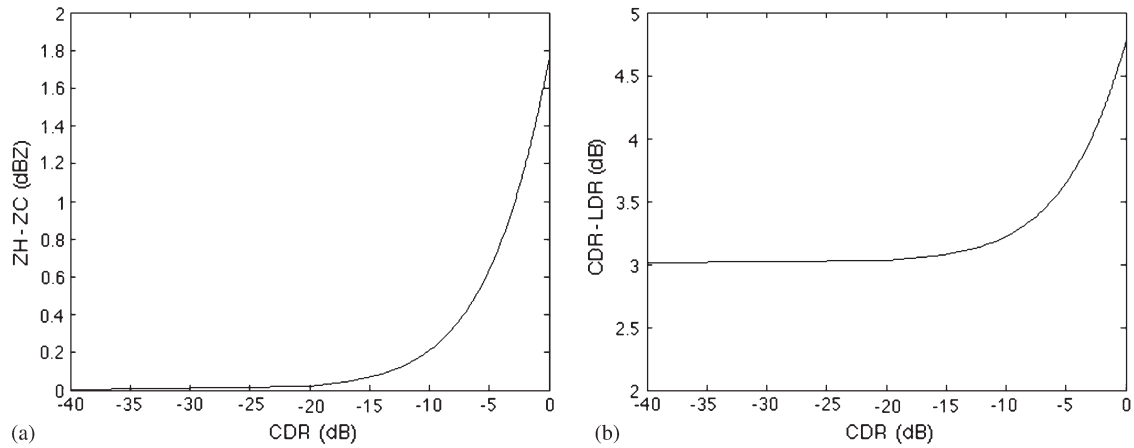

Fig. 2. Case 1, $A_0 \geq B_0$ from spheres to dipoles: On the abscissa is CDR in dB units, ranging from -40 dB (approximately a cloud of spheres) to 0 dB (cloud of dipoles). On the left is the difference between reflectivity at linear and reflectivity at circular polarization, $Z_{\rm H} - Z_{\rm C}$ in dBZ units, on the right is the difference between CDR and LDR in dB. Even though $Z_{\rm H}$ is always larger than $Z_{\rm C}$, the difference is negligible (< 0.2 dBZ) for most atmospheric scatterers (with intrinsic $CDR < -10$ dB); the difference in reflectivity is more significant only for scatterers with $CDR > -5$ dB, and attains its maximum value for a cloud of randomly oriented dipoles, for which the difference is 1.76 dBZ. On the right panel, the difference between CDR and LDR is not negligible, and is larger than 3 dB for every atmospheric scatterer. The difference between CDR and LDR grows larger for scatterers with $CDR > -5$ dB and attains its maximum value for a cloud of randomly oriented dipoles, for which the difference is 4.77 dB.

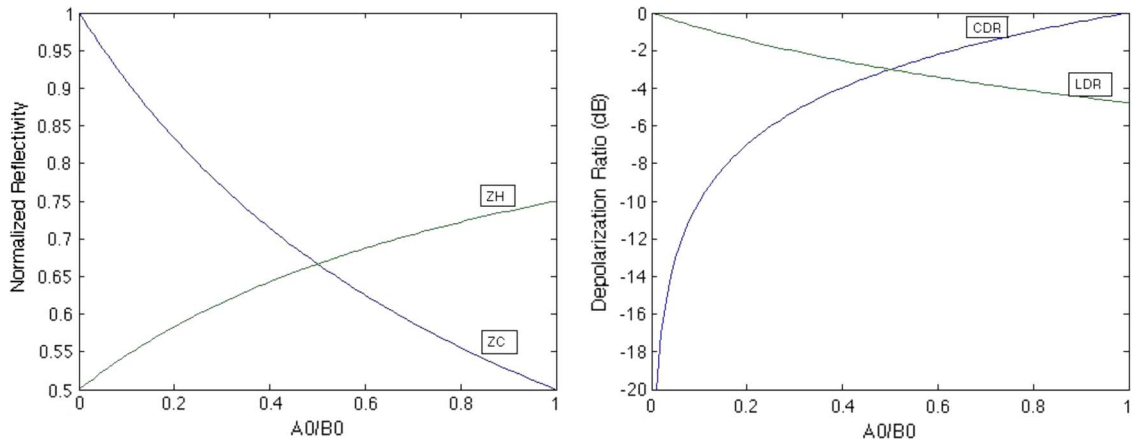

Fig. 3. Case 2, $A_0 < B_0$ from dipoles to helices: On the abscissa is A_0/B_0 (CDR in linear units) ranging from 0 (cloud of helices) to 1 (cloud of dipoles). These types of scatterers are seldom found in the atmosphere. On the left the ordinate is the normalized reflectivity, showing that $Z_{\rm H} = Z_{\rm C}$ for $2A_0 = B_0$. On the right the ordinate is the depolarization ratio, showing that $LDR = CDR$ for $2A_0 = B_0$.

TABLE I
T-MATRIX SIMULATION RESULTS FOR 3-D RANDOMLY ORIENTED SPHEROIDS AT KA BAND, AND FOR 3-D RANDOMLY ORIENTED COLUMNAR CRYSTALS AT KA AND W BANDS

Randomly Oriented	Size	Axis ratio	$Z_H - Z_C$	CDR – LDR
Spheroids - Ka	D = 2 mm	0.83	0.04 dBZ	3.04 dB
Spheroids - Ka	D = 6 mm	0.6	0.13 dBZ	3.15 dB
Columns - Ka	Length = 2 mm	0.2	0.13 dBZ	3.1 dB
Columns - W	Length = 2 mm	0.2	0.27 dBZ	3.33 dB

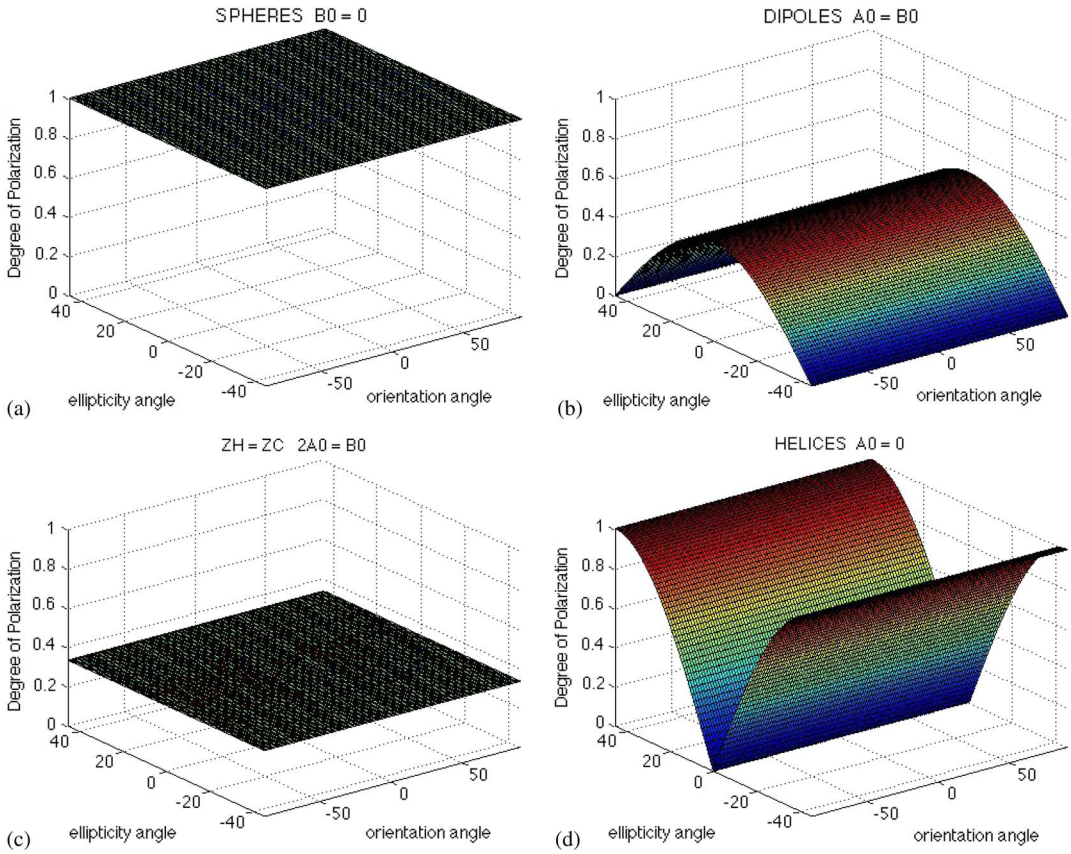

Fig. 4. Degree of Polarization Poincare maps for scatterers with azimuth symmetry: (a) cloud of spheres, (b) cloud of randomly oriented dipoles, (c) cloud of scatterers for which $Z_{\rm H} = Z_{\rm C}$, $LDR = CDR = 0.5$ (linear units) and $\rho_{\rm hv} = 0$, (d) balanced cloud of right-hand and left-hand helices. Note how the degree of polarization at linear transmission goes from 1.00 (a) to 0.50 (b) to 0.33 (c) to 0.00 (d).

$A_0 < B_0$ we have that A_0 varies between 0 and B_0. For $A_0 = B_0$ we obtain again the cloud of dipoles described above. For $A_0 = 0$ we have that [Fig. 4(d)]

$$p(\psi, \chi) = \sin(2\chi). \tag{37}$$

This type of target corresponds to a balanced mixture of right and left helices [3], and in this case the degree of polarization at circular is larger than the degree of polarization at linear. This corresponds to reflectivity at circular larger than reflectivity at linear. Since this situation is the opposite of what we obtain for the cloud of dipoles $(A_0 = B_0)$, we set out to identify where the transition occurs. The degree of polarization at horizontal transmit is given by

$$p_H = \frac{A_0}{A_0 + B_0} \tag{38}$$

from which we have that

$$LDR = \frac{B_0}{2A_0 + B_0} \tag{39}$$

whereas the degree of polarization at circular transmit is given by

$$p_c = \frac{B_0 - A_0}{A_0 - B_0} \tag{40}$$

from which we have

$$CDR = \frac{A_0}{B_0}. \tag{41}$$

The equality is obtained for $2A_0 = B_0$, and this corresponds to a constant degree of polarization Poincare map equal to 1/3

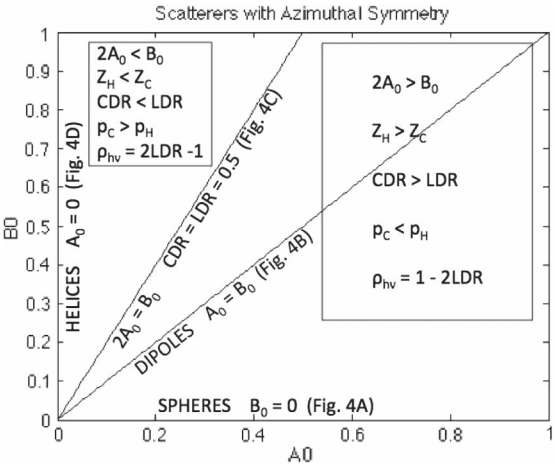

Fig. 5. In the diagram above, the $A_0 - B_0$ plane, we identify the respective loci corresponding to a cloud of spheres ($B_0 = 0$), to a cloud of dipoles ($A_0 = B_0$) and to a cloud of right-hand and left-hand helices ($A_0 = 0$). The line corresponding to $2A_0 = B_0$ marks the transition between scatterers for which reflectivity at linear transmit is larger than reflectivity at circular transmit. Real atmospheric scatterers are generally characterized by $A_0 \gg B_0$ and tend to lie close to the x-axis (spheres).

[Fig. 4(c)]. For scatterers characterized by $2A_0 = B_0$, we note that $CDR = LDR = 0.5$ (linear units), $Z_{\rm H} = Z_{\rm C}$, and $\rho_{\rm hv} = 0$.

Reflectivity at circular polarization is larger than reflectivity at linear polarization only for scatterers with intrinsic LDR (or CDR) larger than 0.5 (linear units). The polarimetric behavior of scatterers with azimuthal symmetry is summarized in Fig. 5, where the $A_0 - B_0$ plane is plotted together with axes corresponding to spheres ($B_0 = 0$), dipoles ($A_0 = B_0$), equal reflectivity axis ($2A_0 = B_0$) and helices (A_0). Obviously, for 2-D plotting, any other choice of parameters is equally suitable, like the couple $Z_{\rm H} - LDR$, or $Z_{\rm C} - CDR$ or Trace and Degree of Polarization plane.

IV. Azimuthal Symmetry: The Dynamic Range of Depolarization Ratio at LDR and CDR Modes

For case 1 analyzed in Section III, that is, the case that generally occurs in the real atmosphere, it was observed that even though reflectivity is comparable at linear and circular transmit, the difference between CDR and LDR is always larger than 3 dB, and tends to exactly 3 dB as the illuminated scatterers tend to the spherical shape [Fig. 2(b)]. Since the upper bound of the depolarization ratio measurements is larger for CDR, it is important to establish the lower bound of both LDR and CDR in order to establish which one of the two variables offers the largest dynamic range.

The lowest measurable depolarization ratio is determined by the antenna cross-polar isolation that, in turn, can be determined by the antenna cross-polar pattern. In this section we assume equal cross-polar patterns for both linear and circular antennas, and set out to compute the bias induced in LDR and CDR in order to establish a theoretical lower bound for such polarimetric variables. The bias in LDR was already computed in [36] and found to be equal to $4W_2$, where W_2 is the second order integrated cross-polar pattern (see [36, eq. (35)]).

In the following, we proceed to the evaluation of the bias in CDR. Assuming reciprocity of the target ($s_{\rm RL} = s_{\rm LR} = s_{\rm x}$) and of the antenna cross-polar patterns ($F_{\rm RL} = F_{\rm LR} = F_{\rm x}$), the received voltages in presence of cross-channel coupling can be expressed as:

$$\begin{bmatrix} V_R \\ V_x \end{bmatrix} = \begin{bmatrix} F_R & F_x \\ F_x & F_R \end{bmatrix} \begin{bmatrix} s_R & s_x \\ s_x & S_L \end{bmatrix} \begin{bmatrix} F_R & F_x \\ F_x & F_R \end{bmatrix} \begin{bmatrix} 1 \\ 0 \end{bmatrix} = \begin{bmatrix} s_R F_R^2 + 2 s_x F_R F_x + s_L F_x^2 \\ s_x F_R^2 + s_L F_R F_x + s_R F_R F_x + s_x F_x^2 \end{bmatrix}. \quad (42)$$

Given azimuthal symmetry, it can be assumed that $\langle |s_{\rm R}|^2 \rangle = \langle |s_{\rm L}|^2 \rangle$, $\langle s_R s_{\rm L}^* \rangle = 0$, $\langle s_R s_{\rm x}^* \rangle = 0$ and $\langle s_{\rm L} s_{\rm x}^* \rangle = 0$.

Hence, the measured copolar and cross-polar powers are found to be:

$$\eta_{\rm R} \equiv \frac{\langle |V_{\rm R}|^2 \rangle}{\langle |s_{\rm x}|^2 \rangle \int_\Omega F_{\rm R}^4} \sim CDR + 4W_2 \quad (43)$$

$$\eta_{\rm x} \equiv \frac{\langle |V_{\rm x}|^2 \rangle}{\langle |s_{\rm x}|^2 \rangle \int_\Omega F_{\rm R}^4} \sim 1 + 2W_2. \quad (44)$$

The intrinsic CDR of the scatterers is defined as:

$$CDR \equiv \frac{\langle |s_{\rm R}|^2 \rangle}{\langle |s_{\rm x}|^2 \rangle}. \quad (45)$$

The second order integrated cross-polar pattern is

$$W_2 = \frac{\int_\Omega F_{\rm R}^2 |F_{\rm x}|^2}{\int_\Omega F_{\rm R}^4}. \quad (46)$$

We finally proceed to the evaluation of the biased CDR:

$$CDR^{\rm B} = \frac{\eta_{\rm R}}{\eta_{\rm x}} \sim \frac{CDR + 4W_2}{1 + 2w_2} \sim CDR + 4W_2 \quad (47)$$

from which follows that the bias is $4W_2$, exactly the same as for LDR (see [36]).

From the above considerations, it is possible to conclude that, for scatterers with azimuthal symmetry, considering two antennas with the same cross-polar isolation, the dynamic range of CDR is always larger than the dynamic range of LDR by at least 3 dB. For anisotropic scatterers (when azimuthal symmetry is broken), the difference between CDR and LDR can be significantly larger than 3 dB [26], and implementation of the CDR mode emerges as an even better option for zenith/nadir pointing mm-wave radars. We emphasize the fact that the depolarization ratio dynamic range is dependent on its minimum measurable value, driven by the antenna cross-polar isolation. The latter can in general be different for linear and circular polarizations [25].

V. Azimuthal Symmetry: Simultaneous Transmission

The analysis carried out so far for scatterers with azimuth symmetry reveals that their scattering behavior can be fully described by two radar variables, one power-related, like

$Z_{\rm H}, Z_{\rm C}$ or the trace of the Coherency matrix, plus one power-independent variable that can equivalently be chosen among LDR, CDR, $p_{\rm H}$, $p_{\rm C}$ or $\rho_{\rm hv}$. In Section III, we investigated the relations among variables at LDR and CDR modes. In this section we extend our analysis to include polarimetric variables obtained at simultaneous transmission. These results are important since some ARM scanning radars are currently designed to operate at simultaneous transmission (e.g., X-SACR), and comparisons of polarimetric measurements at zenith from different radar architectures are important for both calibration and retrieval purposes.

This analysis also applies to cm-wavelength scanning precipitation radars operating at simultaneous transmission and illuminating scatterers with azimuthal symmetry, the latter characterized by differential reflectivity $Z_{\rm DR} = 0$ dB and backscatter copolar phase $\delta co = 0^\circ$. As an example, hail or graupel may have azimuthal symmetry, but they may also depart from it with large δco and non-zero $Z_{\rm DR}$ values. For hail and/or graupel with azimuthal symmetry, the copolar correlation coefficient $\rho_{\rm hv}$ remains the only degree of freedom left to characterize their shape.

In this section, we theoretically derive a relation that links the degree of polarization at simultaneous transmission (measured at some point on the circular/slant circle of the Poincare sphere) with any of the aforementioned power-independent variables (LDR, CDR, $p_{\rm H}$, $p_{\rm C}$, or $\rho_{\rm hv}$). The results are important for shape characterization, since the copolar correlation coefficient measured at STSR mode is generally biased by the non-zero cross-polar return of the target (intrinsic LDR > 0), and because none of the other power-independent variables (LDR, CDR, $p_{\rm H}$) is available at STSR mode. The procedure outlined in the present section permits to account for differential propagation phase effects: if this problem is negligible for zenith/nadir pointing mm-wavelength radars, the same may not occur for scanning cm-wavelength radars, since scatterers with azimuth symmetry (tumbling hailstones or graupel for example) are often embedded in rain that induces a propagation phase. Contrary to CDR or ORTT for example, both positively biased by propagation through rain, the degree of polarization at circular polarization $p_{\rm C}$ (or, in general, at simultaneous transmission $p_{\rm S}$) is not strongly dependent on differential phase when anisotropic scatterers (rain) are illuminated (see [37]). However, for a target with azimuth symmetry, the degree of polarization at simultaneous transmission is crucially dependent on the specific polarization state (lying on the circular/slant circle of the Poincare sphere) that impinges on the hydrometeors [37].

Radars operating at Simultaneous Transmission measure the Coherency matrix

$$\mathbf{J}_{\boldsymbol{\chi}}^{\mathbf{HV}} \equiv \begin{bmatrix} \langle |s_{\rm h\chi}|^2 \rangle & \langle s_{\rm h\chi} s_{\rm v\chi}^* \rangle \\ \langle s_{\rm v\chi} s_{\rm h\chi}^* \rangle & \langle |s_{\rm v\chi}|^2 \rangle \end{bmatrix} \tag{48}$$

where the subscript χ indicates the transmit polarization state (lying on the circular/slant circle of the Poincare sphere, corresponding to simultaneous transmission of H and V) and the superscript HV indicates simultaneous reception of horizontal and vertical polarizations. For a general target with scattering matrix $\mathbf{S}$

$$\mathbf{S} = \begin{bmatrix} s_{\rm hh} & s_{\rm hv} \\ s_{\rm vh} & s_{\rm vv} \end{bmatrix}. \tag{49}$$

The entries of the Coherency matrix at Simultaneous Transmission can be expressed as:

$$\begin{aligned} \mathbf{J}_{\boldsymbol{\chi}}^{\mathbf{HV}} &\equiv \begin{bmatrix} \langle |s_{\rm h\chi}|^2 \rangle & \langle s_{\rm h\chi} s_{\rm v\chi}^* \rangle \\ \langle s_{\rm v\chi} s_{\rm h\chi}^* \rangle & \langle |s_{\rm v\chi}|^2 \rangle \end{bmatrix} \\ &= \begin{bmatrix} \langle |s_{\rm hh}+s_{\rm hv}|^2 \rangle & \langle (s_{\rm hh}+s_{\rm vv})(s_{\rm vv}+s_{\rm vh})^* \rangle \\ \langle (s_{\rm vv}+s_{\rm vh})(s_{\rm hh}+s_{\rm hv})^* \rangle & \langle |s_{\rm vv}+s_{\rm vh}|^2 \rangle \end{bmatrix}. \end{aligned} \tag{50}$$

From the matrix $\mathbf{J}_{\boldsymbol{\chi}}^{\rm HV}$, reflectivity $(Z_{\rm H}^{\rm S})$, differential reflectivity $(Z_{\rm DR}^{\rm S})$, copolar correlation coefficient $(\rho_{\rm hv}^{\rm s})$, degree of polarization at simultaneous transmission $(p_{\rm s})$ and differential phase $(\Phi_{\rm hv}^{\rm s} + \delta_{\rm hv}^{\rm s}))$ can be evaluated for radars operating at hybrid mode:

$$Z_{\rm H}^{\rm S} \propto \langle |s_{\rm h\chi}|^2 \rangle \tag{51}$$

$$Z_{\rm DR}^{\rm S} \equiv \frac{\langle |s_{\rm h\chi}|^2 \rangle}{\langle |s_{\rm v\chi}|^2 \rangle} \tag{52}$$

$$\rho_{\rm hv}^{\rm S} = \frac{\left| \langle s_{\rm h\chi} s_{\rm v\chi}^* \rangle \right|}{\sqrt{\langle |s_{\rm h\chi}|^2 \rangle \langle |s_{\rm v\chi}|^2 \rangle}} \tag{53}$$

$$\left(\Phi_{\rm hv}^{\rm S} + \delta_{\rm hv}^{\rm S}\right) \equiv \arg \langle s_{\rm h\chi} s_{\rm v\chi}^* \rangle \tag{54}$$

$$P_{\rm s} = \sqrt{1 - \frac{4 \det \left[\mathbf{J}_{\boldsymbol{\chi}}^{\mathbf{HV}}\right]}{\left(\mathrm{trace}\left[\mathbf{J}_{\boldsymbol{\chi}}^{\mathbf{HV}}\right]\right)^2}} = \frac{\lambda_1 - \lambda_2}{\lambda_1 + \lambda_2} \tag{55a}$$

$$trace\left[\mathbf{J}_{\boldsymbol{\chi}}^{\rm HV}\right] \equiv \langle |s_{\rm h\chi}|^2 \rangle + \langle |s_{\rm v\chi}|^2 \rangle = \lambda_1 + \lambda_2 \tag{55b}$$

$$\begin{aligned} \det\left[\mathbf{J}_{\boldsymbol{\chi}}^{\rm HV}\right] &\equiv \langle |s_{\rm h\chi}|^2 \rangle \langle |s_{\rm v\chi}|^2 \rangle - \langle s_{\rm h\chi} s_{\rm v\chi}^* \rangle \\ &= \lambda_1 \cdot \lambda_2. \end{aligned} \tag{55c}$$

In (55), λ_1 and λ_2 are the eigenvalues of $\mathbf{J}_{\boldsymbol{\chi}}^{\mathbf{HV}}$.

Simultaneous transmission implies that in presence of intrinsically cross-polarizing scatterers $(s_{\rm hv} > 0)$, differential reflectivity and copolar correlation coefficient will differ from the corresponding variables measured at Alternate Transmit and Simultaneous Reception mode (ATSR mode) [1]

$$\begin{aligned} \rho_{\rm hv}^{\rm s} &\equiv \frac{|\langle (s_{\rm hh}+s_{\rm hv})(s_{\rm vv}+s_{\rm vh})^* \rangle|}{\sqrt{\langle |s_{\rm hh}+s_{\rm hv}|^2 \rangle \langle |s_{\rm vv}+s_{\rm vh}|^2 \rangle}} \neq \frac{|\langle s_{\rm hh} s_{\rm vv}^* \rangle|}{\sqrt{\langle |s_{\rm hh}|^2 \rangle \langle |s_{\rm vv}|^2 \rangle}} \\ &\equiv \rho_{\rm hv} \end{aligned} \tag{56}$$

$$Z_{\rm DR}^{\rm S} \equiv \frac{\langle |s_{\rm hh}+s_{\rm vv}|^2 \rangle}{\langle |s_{\rm vv}+s_{\rm vh}|^2 \rangle} \neq \frac{\langle |s_{\rm hh}|^2 \rangle}{\langle |s_{\rm vv}|^2 \rangle} \equiv Z_{\rm DR}. \tag{57}$$

For scatterers with azimuth symmetry (virtually any atmospheric scatterers in zenith/nadir geometry, or, for scanning precipitation radars, hail and graupel with $Z_{\rm DR} = 0$ dB and

$\delta co = 0^\circ$), the degree of polarization Poincare map is in general given by (58), that we report here for simplicity

$$p(\psi, \chi) = \frac{\sqrt{A_0^2 \cos^2(2\chi) + (A_0 - B_0)^2 \sin^2(2\chi)}}{A_0 + B_0}. \quad (58)$$

We note how the differential propagation phase $\Phi_{\rm hv}^{\rm s}$ can be measured independently, and, together with the system differential phase β, they provide a precise indication about the actual polarization state impinging on the azimuth symmetric hydrometeors. If we plug the propagation differential phase and the system differential phase in (58), we can relate the degree of polarization measured at simultaneous transmission with the parameters A_0 and B_0:

$$p\left(45^\circ, \frac{\beta + \Phi_{\rm hv}^{\rm s}}{2}\right) = \frac{\sqrt{A_0^2 \cos^2(\beta + \Phi_{\rm hv}^{\rm s}) + (A_0 - B_0)^2 \sin^2(\beta + \Phi_{\rm hv}^{\rm s})}}{A_0 + B_0}. \quad (59)$$

In general, for any type of target, the trace of the covariance matrix is invariant with respect to a change of polarization basis. For scatterers with azimuth symmetry, not only the trace of the covariance matrix, but also the trace of the Coherency matrix (measured by a dual-polarization system) is invariant for a change of polarization bases. The important consequence is that, for scatterers with azimuth symmetry, the trace of the Coherency matrix is the same at simultaneous transmission, LDR mode or CDR mode, and is equal to $(A_0 + B_0)$

$$\begin{aligned} trace\left[\mathbf{J}_{\boldsymbol{\chi}}^{\rm HV}\right] &= Z_H^S \left[1 + Z_{DR}^{S^{-1}}\right] = Z_H[1 + LDR] \\ &= Z_C[1 + CDR] = A_0 + B_0. \end{aligned} \quad (60)$$

Equations (59) and (60) can be combined to form a system whose solution yields A_0 and B_0. These latter parameters can then be used to evaluate any of the following polarimetric variables: LDR, CDR, $p_{\rm H}$, $p_{\rm C}$ or $\rho_{\rm hv}$. Note that the copolar correlation coefficient derived with this procedure is not affected by the bias due to cross-polarizing scatterers (with $s_{\rm hv} > 0$), that, in turn, affects the copolar correlation coefficient measured at simultaneous transmission: $\rho_{\rm hv}^{\rm s}$ [38].

VI. Conclusion

The paper presents a consistent theoretical framework for the analysis of polarimetric signatures from zenith/nadir-pointing atmospheric radars at LDR, CDR, and $Z_{\rm DR}$ modes.

Under the assumption of azimuthal symmetry, we show that

1) The difference in reflectivity between radars at LDR and CDR modes is generally negligible: $Z_{\rm H} - Z_{\rm C}$ is less than 0.5 dBZ for scatterers with intrinsic $CDR < -6$ dB.
2) The difference in depolarization ratio (i.e., the difference between CDR and LDR) is always larger than 3 dB and is non-negligible. Assuming antennas with the same cross-polar isolation (ICPR), CDR mode offers a dynamic range that is larger by at least 3 dB.

With no azimuthal symmetry, that is, in presence of aligned scatterers in the polarization plane (e.g., insects or electrified crystals), contrary to all variables obtained at LDR mode, variables obtained at CDR mode are not affected by the specific alignment direction of the scatterers with respect to the antenna ports. When measured at CDR mode, reflectivity, depolarization ratio, cross-polar coherence and degree of polarization are invariant with respect to rotations about the boresight axis. In particular, in presence of anisotropic (aligned) scatterers, the dynamic range of CDR may be larger than the dynamic range of LDR by more than 10 dB [26].

For zenith/nadir pointing dual-polarization atmospheric radars, implementation of the CDR mode might be preferable with respect to the LDR mode for two reasons:

- Larger dynamic range of the depolarization ratio (valid for scatterers with and without azimuthal symmetry, assuming equal antenna cross-polar isolation)
- Rotational invariance of the retrieved variables (in case scatterers without azimuthal symmetry are present)

In Section V, we only consider scatterers with azimuthal symmetry, and we derive a set of two algebraic equations [namely (59) and (60)] that relate variables obtained at LDR and CDR modes with variables obtained at simultaneous transmission: these theoretical results are applicable not only to zenith/nadir pointing mm-wavelength radars (Ka, W bands), but also to scanning cm-wavelength radars (S, C, X bands) whenever scatterers with azimuthal symmetry (e.g., dry hail or graupel with $Z_{\rm DR} = 0$ dB and $\delta_{\rm co} = 0^\circ$) are illuminated, and may be used to evaluate estimates of the copolar correlation coefficient $\rho_{\rm hv}$ that are unbiased by intrinsically cross-polarizing scatterers (with $s_{\rm hv} > 0$).

References

[1] V. N. Bringi and V. Chandrasekhar, *Polarimetric Doppler Weather Radar: Principles and Applications*. Cambridge, U.K.: Cambridge Univ. Press, 2001.

[2] R. J. Doviak and D. S. Zrnic, *Doppler Radar and Weather Observations*., 2nd ed. San Diego, CA, USA: Academic, 1993.

[3] J.-S. Lee and E. Pottier, *Polarimetric Radar Imaging, From Basics to Applications*. Boca Raton, FL, USA: CRC Press, 2009.

[4] T. Ackerman and G. M. Stokes, "The atmospheric radiation measurement program," *Phys. Today*, vol. 56, no. 1, pp. 38–45, Jan. 2003.

[5] P. Kollias, M. A. Miller, E. P. Luke, K. L. Johnson, E. E. Clothiaux, K. P. Moran, K. B. Widener, and B. A. Albrecht, "The atmospheric radiation measurement program cloud profiling radars: Second-generation sampling strategies, processing, cloud data products," *J. Atmos. Ocean. Technol.*, vol. 24, no. 7, pp. 1199–1214, Jul. 2007.

[6] K. P. Moran, B. E. Martner, M. J. Post, R. A. Kropfli, D. C. Welsh, and K. B. Widener, "An unattended cloud-profiling radar for use in climate research," *Bull. Amer. Meteorol. Soc.*, vol. 79, no. 3, pp. 443–455, Mar. 1998.

[7] S. Y. Matrosov, G. G. Mace, R. Marchand, M. D. Shupe, A. G. Hallar, and I. B. McCubbin, "Observations of ice crystal habits with a scanning polarimetric W-band radar at slant linear depolarization ratio mode," *J. Atmos. Ocean. Technol.*, vol. 29, no. 8, pp. 989–1008, Aug. 2012.

[8] S. Y. Matrosov, "Prospects for the measurement of ice particle shape and orientation with elliptically polarized radar signals," *Radio Sci.*, vol. 26, no. 4, pp. 847–856, Jan. 1991.

[9] R. F. Reinking, S. Y. Matrosov, R. A. Kropfli, and B. W. Bartram, "Evaluation of a 45 ° slant quasi-linear radar polarization state for distinguishing drizzle droplets, pristine ice crystals, less regular ice particles," *J. Atmos. Ocean. Technol.*, vol. 19, no. 3, pp. 296–321, Mar. 2002.

[10] A. Ryzhkov, D. S. Zrnic, J. C. Hubbert, V. N. Bringi, J. Vivekanandan, and E. A. Brandes, "Polarimetric radar observations and interpretation of co-cross-polar correlation coefficients," *J. Atmos. Ocean. Technol.*, vol. 19, no. 3, pp. 340–354, Mar. 2002.
[11] A. V. Ryzhkov, "Interpretation of polarimetric radar covariance matrix for meteorological scatterers: Theoretical analysis," *J. Atmos. Ocean. Technol.*, vol. 18, no. 3, pp. 315–328, Mar. 2001.
[12] S. V. Nghiem, S. H. Yueh, R. Kwok, and F. K. Li, "Symmetry properties in polarimetric remote sensing," *Radio Sci.*, vol. 27, no. 5, pp. 693–711, Jan. 1992.
[13] C. Tang and K. Aydin, "Scattering from ice crystals at 94 and 220 GHz millimeter wave frequencies," *IEEE Trans. Geosci. Remote Sens.*, vol. 33, no. 1, pp. 93–99, Jan. 1995.
[14] K. Aydin and C. Tang, "Millimeter wave radar scattering from model ice crystal distributions," *IEEE Trans. Geosci. Remote Sens.*, vol. 35, no. 1, pp. 140–146, Jan. 1997.
[15] K. Aydin and C. Tang, "Relationships between IWC and polarimetric radar measurands at 94 and 220 GHz for hexagonal columns and plates," *J. Atmos. Ocean. Technol.*, vol. 14, no. 5, pp. 1055–1063, Oct. 1997.
[16] G. Botta, K. Aydin, and J. Verlinde, "Modeling of microwave scattering from cloud ice crystal aggregates and melting aggregates: A New Approach," *IEEE Geosci. Remote Sens. Lett.*, vol. 7, no. 3, pp. 572–576, Jul. 2010.
[17] A. R. Jameson and S. L. Durden, "A possible origin of linear depolarization observed at vertical incidence in rain," *J. Appl. Meteorol.*, vol. 35, no. 2, pp. 271–277, Feb. 1996.
[18] K. V. Beard, "Oscillation models for predicting raindrop axis and backscatter ratios," *Radio Sci.*, vol. 19, no. 1, pp. 67–74, Jan./Feb. 1984.
[19] F. Y. Testik, A. P. Barros, and L. F. Bliven, "Field observations of multimode raindrop oscillations by high-speed imaging," *J. Atmos. Sci.*, vol. 63, no. 10, pp. 2663–2668, Oct. 2006.
[20] F. Y. Testik, A. P. Barros, and L. F. Bliven, "Toward a physical characterization of raindrop collision outcome regimes," *J. Atmos. Sci.*, vol. 68, no. 5, pp. 1097–1113, May 2011.
[21] M. Galletti, D. Huang, P. Kollias, and S. E. Giangrande, "Towards a CDR-based rain rate estimation algorithm for Zenith-pointing cloud radars at Ka band," in *Proc. 7th ERAD Conf. Meteorol. Hydrol.*, Toulouse, France, Jun. 24–29, 2012. [Online]. Available: www.meteo.fr/cic/meetings/2012/ERAD/extended_abs/CR_100_ext_abs.pdf
[22] B. E. Martner and K. P. Moran, "Using cloud radar polarization measurements to evaluate stratus cloud and insect echoes," *J. Geophys. Res.*, vol. 106, no. D5, pp. 4891–4897, Jan. 2011.
[23] E. P. Luke, P. Kollias, K. L. Johnson, and E. E. Clothiaux, "A technique for the automatic detection of insect clutter in cloud radar returns," *J. Atmos. Ocean. Technol.*, vol. 25, no. 9, pp. 1498–1513, Sep. 2008.
[24] G. C. McCormick, "Polarization errors in a two-channel system," *Radio Sci.*, vol. 16, no. 1, pp. 67–75, Jan. 1981.
[25] T.-S. Chu and R. Turrin, "Depolarization properties of offset reflector antennas," *IEEE Trans. Antennas Propag.*, vol. AP-21, no. 3, pp. 339–345, May 1973.
[26] E. Torlashi and A. R. Holt, "A comparison of different polarization schemes for the radar sensing of precipitation," *Radio Sci.*, vol. 33, no. 5, pp. 135–1352, Jan. 1998.
[27] Y. Wang and V. Chandrasekar, "Polarization isolation requirements for linear dual-polarization weather radar in simultaneous transmission mode of operation," *IEEE Trans. Geosci. Remote Sens.*, vol. 44, no. 8, pp. 2019–2028, Aug. 2006.
[28] J. C. Hubbert, S. M. Ellis, M. Dixon, and G. Meymaris, "Modeling, error analysis, evaluation of dual-polarization variables obtained from simultaneous horizontal and vertical polarization transmit radar I: Modeling and Antenna Errors," *J. Atmos. Ocean. Technol.*, vol. 27, no. 10, pp. 1583–1598, Oct. 2010.
[29] J. C. Hubbert, S. M. Ellis, M. Dixon, and G. Meymaris, "Modeling, error analysis, evaluation of dual-polarization variables obtained from simultaneous horizontal and vertical polarization transmit radar II: Experimental Data," *J. Atmos. Ocean. Technol.*, vol. 27, no. 10, pp. 1599–1607, Oct. 2010.
[30] J. C. Hubbert, S. M. Ellis, M. Dixon, and G. Meymaris, "Antenna polarization errors and biases in polarimetric variables for simultaneous horizontal and vertical transmit radar," in *Proc. 6th ERAD Conf. Meterol. Hydrol.*, Sibiu, Romania, pp. 1–6.
[31] A. V. Ryzhkov, "The impact of beam broadening on the quality of radar polarimetric data," *J. Atmos. Ocean. Technol.*, vol. 24, no. 5, pp. 729–744, May 2007.
[32] M. I. Mishchenko and L. D. Travis, "Capabilities and limitations of a current FORTRAN implementation of the T-matrix method for randomly oriented, rotationally symmetric scatterers," *J. Quant. Spectrosc. Radiat. Transf.*, vol. 60, no. 3, pp. 309–324, Sep. 1998.
[33] M. I. Mishchenko, L. D. Travis, and D. W. Mackowski, "T-matrix method and its applications to electromagnetic scattering by particles: A current perspective," *J. Quant. Spectrosc. Radiat. Transf.*, vol. 111, no. 11, pp. 1700–1703, Jul. 2010.
[34] M. I. Mishchenko and L. Liu, "Electromagnetic scattering by densely packed particulate ice at radar wavelengths: Exact theoretical results and remote sensing implications," *Appl. Opt.*, vol. 48, no. 13, pp. 2421–2426, May 2009.
[35] E. Wolf, "Coherence Properties of Partially Polarized Electromagnetic Radiation," *Il Nuovo Cimento*, vol. 13, no. 6, pp. 1165–1181, Sep. 1959.
[36] M. Galletti, D. S. Zrnic, V. M. Melnikov, and R. J. Doviak, "Degree of polarization at horizontal transmit: Theory and applications for weather radar," *IEEE Trans. Geosci. Remote Sens.*, vol. 50, no. 4, pp. 1291–1301, Apr. 2012.
[37] M. Galletti, D. H. O. Bebbington, M. Chandra, and T. Boerner, "Measurement and characterization of entropy and degree of polarization of weather radar targets," *IEEE Trans. Geosci. Remote Sens.*, vol. 46, no. 10, pp. 3196–3207, Oct. 2008.
[38] M. Galletti and D. S. Zrnic, "Degree of polarization at simultaneous transmit: Theoretical aspects," *IEEE Geosci. Remote Sens. Lett.*, vol. 9, no. 3, pp. 383–387, May 2012.
[39] S. Y. Matrosov, "Depolarization estimates from linear H and V measurements with weather radars operating in simultaneous transmission-simultaneous receiving mode," *J. Atmos. Ocean. Technol.*, vol. 21, no. 4, pp. 574–583, Apr. 2004.

Michele Galletti was born in Bologna, Italy. He received the Ph.D. degree in electrical engineering from the Microwave Engineering Department, Technische Universitaet Chemnitz (funded by the European Commission through the AMPER project) and also with the Microwaves and Radar Institute of the German Aerospace Center (DLR-HR in Oberpfaffenhofen, Germany).

In 2009, he was awarded a National Research Council Post-doctoral position at the National Severe Storms Laboratory in Norman, OK. During this period, he worked on projects related to polarimetric phased array weather radars. He is a member of the Radar Science Group at BNL. His research interests cover a wide span of weather and climate radar science topics at many frequencies (S, C, X, Ka, W, and beyond), with a focus on the theory and applications of radar polarimetry for atmospheric remote sensing.

Dong Huang scientific career has been centered on radiation transfer/particle transport in complex medium. This interest began while he was a college student at Beijing Normal University where he took a course about Monte Carlo simulations of ion implantation. This was continued at Boston University when he developed a stochastic radiative transfer theory for 3D vegetation canopies with Profs. Yuri Knyazikhin and Ranga Myneni. The resultant theory became the basis of the forward model of the operational MODIS Leaf Area Index and Fraction of Photosynthetically Active Radiation retrievals. Since joining BNL, he has been working on remote sensing of clouds and representing small-scale cloud variability in climate models. Several novel techniques have been developed, including cloud tomography and multi-frequency cloud radar, to improve measurements of 3D clouds. He is also involved in a cloud nowcasting project in support of the operation of the largest PV solar farm in the Eastern United States.

Pavlos Kollias was born in Athens, Greece, in 1971. He received the B.Sc. degree in physics and the M.Sc. degree in environmental physics from the University of Athens, Athens, Greece, in 1994 and 1996, respectively, and the Ph.D. degree in meteorology from the University of Miami, Miami in 2000.

Currently, he is an Associate Professor and Canada Research Chair in Radar Application in Weather and Climate Research at the Department of Atmospheric and Oceanic Sciences, McGill University, Canada. He is an international leader in the application of short wavelength radars for cloud and precipitation research from ground- and space-based platforms. He has published over 60 scientific articles in peer-reviewed literature in the areas of millimeter wavelength radar research, cloud, and precipitation physics. He is a member of the Mission Advisory Group and algorithm development team of the European Space Agency Earth Clouds Aerosols Radiation Experiment (EARTHCARE) Explorer Mission and the leader of the DOE Atmospheric Systems Research (ASR) radar science group. He has served as a member at the National Science Foundation Engineering Research Center for the Collaborative Adaptive Sensing of the Atmosphere and as Associate Chief Scientist for the US DOE Atmospheric Radiation Measurements program, the largest climate research program in the United States. He has participated in several international satellite mission concepts (e.g., SnowSat, Polar Precipitation Mission, and StormSat) proposed to space agencies in Canada, United States, and Europe. He has served as the Chair of the American Meteorological Society (AMS) Committee on Radar Meteorology and has organized and chaired numerous sessions in AMS, AGU, and ASR conferences.